72nd International Astronautical Congress, Dubai, United Arab Emirates, 25-29 October 2021.

IAC–21–D3.2A.6

CISLUNAR DISTRIBUTED ARCHITECTURES FOR COMMUNICATION AND NAVIGATION SERVICES OF LUNAR ASSETS

Andrea Pasquale,[*,a] **Giovanni Zanotti,**[b] **Jacopo Prinetto,**[c] **Michele Ceresoli,**[d] **Michèle Lavagna**[e]

[a]*Dipartimento di Scienze e Tecnologie Aerospaziali, Politecnico di Milano, Via La Masa, 34, 20156 Milano - Italy*
[b]*Dipartimento di Scienze e Tecnologie Aerospaziali, Politecnico di Milano, Via La Masa, 34, 20156 Milano - Italy*
[c]*Dipartimento di Scienze e Tecnologie Aerospaziali, Politecnico di Milano, Via La Masa, 34, 20156 Milano - Italy*
[d]*Dipartimento di Scienze e Tecnologie Aerospaziali, Politecnico di Milano, Via La Masa, 34, 20156 Milano - Italy*
[e]*Dipartimento di Scienze e Tecnologie Aerospaziali, Politecnico di Milano, Via La Masa, 34, 20156 Milano - Italy*

[*] Corresponding Author

The last decade saw a renewed interest on the Moon as a well suited training premise in preparation to manned mission to Mars, but also as an interesting target itself, for scientific investigations, technological developments and new markets opportunities. As a result, numerous and very different missions to the Moon are currently being studied and implemented, assuming to have our satellite quite crowded soon.
Such a scenario motivates the settling of space infrastructures to offer recurrent services like data relays, communication links and navigation in the cislunar environment which would facilitate and enlighten the single mission's implementation and operation.
The paper presents the strategy adopted to address the design of the orbital configuration for a distributed architecture to answer the communication and navigation needs to serve at the best the diversified lunar missions scenario expected for the next decades. First, a set of parameters of merit are identified and explained in their mathematical expression and physical meaning. Then, different regions of interest for possible future missions are identified and mapped to the relevant performances wanted for that specific region. Last a Multi-Objective Optimisation framework is presented, both in the exploited genotype and the different objectives participating to the definition of the cost function, in order to provide a versatile tool.
The paper critically discusses the effectiveness of the proposed approach in detecting the best suited distributed orbital architectures for the servicers according to the expected service performance in specific user regions, spread all over the Earth-Moon volume - from Earth vicinity to Lunar surface, considering also robustness aspects. The benefits in the exploitation of the multibody dynamical regime offered by the Earth-Moon system to set up the most promising orbital set with a minimum number of servicing spacecraft are underlined as well.

Keywords: Constellation, Communication, GNSS, Non-Keplerian Orbits, Moon South-Pole, Cislunar Space

1. Introduction

Many if not all human-related activities on the Earth rely on by space-related infrastructures which are able to provide high-quality services for both communication and navigation purposes. An example of the former is found in the satellite TV broadcasting or the satellite telephone services, which allow real-time transmission of a wide range of datarate signals between terminals located in different and not in mutual visibility sites. For the latter instead, nowadays all the technological personal devices are equipped with GNSS receivers in order to estimate the position of the terminal on the globe with precisions in the order of the metres or less. There is no doubt that these are key-enabling technologies for the development and support of many activities and functions that years ago were not even imaginable.

The next decades will see a continuous and renewed interest towards our natural satellite, which will be declined into a series of Lunar exploration mission, with particular attentions to surface assets such as landers, rovers and even humans [14]. Particularly, given some specific features of the orography and mineralogy, the South Pole region will be for certain one of the most targeted spots on the surface [5, 7, 8, 21].

With this perspective in mind, the possibility of exploiting communication and navigation infrastructures on the Moon surface would be revolutionary for the enabling of specific exploration activities that require real-time operations from the Earth and precise positioning on-board. In particular, two services would be necessary:

- continuous time windows of Earth-Moon *Communication* relay;
- surface GNSS-like *Navigation* service for positioning.

In order to do that a satellite constellation can be put in place. There are already a number of studies [6, 10, 11] that propose different constellations architectures exploiting both Keplerian and non-Keplerian orbits. However, meeting specific performances on different regions of the Moon surface can be challenging. For such reason, the current paper proposes an innovative approach to extract optimal solutions from a specific set of constraints and performance requirements.

Following this brief introduction, Section 2 will present the mathematical translation of the key performance indexes involved in the constellation design. After that, Section 3 will provide an overview of the defined optimisation strategy architecture, together with all the rationale behind such selection. The results of some exemplary optimisation runs are discussed in Section 4, where among three possible optima, more simulations are conducted to assess the robustness of the constellations to failure. Additionally, in Section 5 the advantages of employing the non-Keplerian orbital regime for one or more additional orbiters of the constellation are described in details. Finally some take-home messages and possible future development are collected in Section 6.

2. Background

2.1 *Visibility & Coverage*

The surface coverage serves as a key parameter both in orbit and constellation design. In fact, it can be used to determine the number of the required satellites to serve a specific surface region, the whole Moon surface or orbital regions in the Moon proximity as well as some other important geometrical visibility aspects.

2.1.1 *Single-sat Coverage*

Considering the Moon surface as a discrete set of m points, P_j, the point-to-point visibility to the i-th satellite S_i can be simply computed in the local horizontal reference frame of P_j. With reference to Fig. 1, if a East-North-Up (ENU) reference frame is assigned to P_j, the elevation angle $\theta_{i,j}$ formed with the satellite S_i can be defined as:

$$\theta_{i,j} = \arcsin \frac{s_z}{|\mathbf{s}|} \quad \text{where} \quad \mathbf{s} = \mathbf{r}_i - \mathbf{u}_j \qquad [1]$$

as far as $\mathbf{s}$ is expressed in the ENU frame. Thus, the visibility function from the i-th satellite to the j-th point could be defined by:

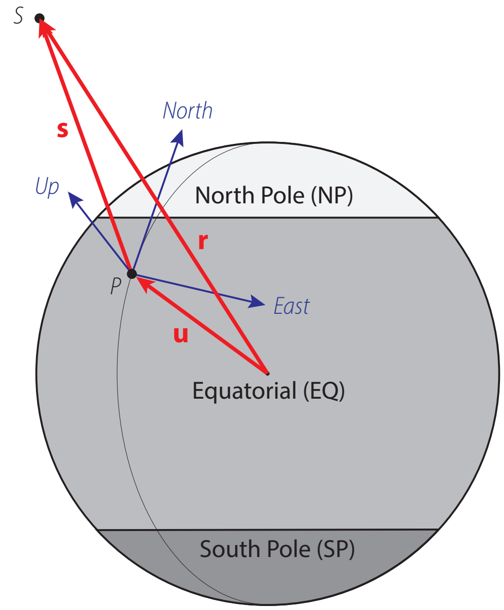

Fig. 1: Moon surface user regions & relative geometry.

$$\mathscr{V}_{i,j}(t) = \begin{cases} 1 & \theta_{i,j}(t) \geq \theta_{\min} \\ 0 & \theta_{i,j}(t) < \theta_{\min} \end{cases} \qquad [2]$$

2.1.2 *Multi-sat Coverage*

In case the coverage function of a j-th point is computed with respect to the whole satellite constellation, the point-to-point satellite visibility functions $\mathscr{V}_{i,j}(t)$ of the constellation must be combined. In particular, having defined the multi-sat coverage function, $\mathscr{N}_j(t)$:

$$\mathscr{N}_j(t) = \sum_i^N \mathscr{V}_{i,j}(t) \quad \text{s.t.} \quad \mathscr{N}_j : \mathbb{R} \rightarrow \mathbb{N} \qquad [3]$$

the *n-fold continuous coverage index* can be defined as:

$$\mathscr{F}_j(t,n) = \begin{cases} 1 & \mathscr{N}_j(t) \geq n \\ 0 & \mathscr{N}_j(t) < n \end{cases} \qquad [4]$$

Moreover, the *n-fold coverage rate* of the j-th surface point can be defined as:

$$\mathscr{C}_j(n) = \frac{\displaystyle\int_{t_0}^{t_f} \mathscr{C}_j(\tau,n)\, d\tau}{t_f - t_0} \qquad [5]$$

Finally, the constellation *Time of Visibility (TOV)* with respect to a point P_j on the Moon surface is simply defined as:

$$\mathtt{TOV}_j = \mathscr{C}_j(1) \qquad [6]$$

Thus, it represents the total time fraction in which at least a single satellite of the constellation is in view of P_j. Indeed, the k-th region Mean Time of Visibility is defined as the mean TOV over a group of N_k surface points, such that:

$$\mathtt{TOV} = \frac{1}{N_k}\sum_{j}^{N_k} \mathtt{TOV}_j \quad [7]$$

2.2 *Dilution of Precision (DOP)*

The concept of DOP is the idea that the position error that results from measurement errors depends on the user relative geometry. The DOP figures therefore represents a key parameter for the evaluation of satellite constellation's navigation performances.

2.2.1 *Pseudo-range Equation Linearization*

The formal derivation of the DOP relations begins with the linearization of the pseudo-range equation [12]. In particular, with reference to Fig. 1, the pseudo-range equation can be written as:

$$\rho = ||\mathbf{s}-\mathbf{u}|| + c\,t_u = f(x_u, y_u, z_u, t_u) \quad [8]$$

where $\mathbf{s}$ is the satellite position of the satellite with respect to the coordinate origin, $\mathbf{u}$ the user position on the body surface, t_u the advance of the receiver clock with respect to the GNSS system time and c the speed of light. In order to determine the user position in three dimensions (x_u, y_u, z_u) as well as the offset t_u, a minimum of 4 pseudo-range measurements are used.

In order to recover the DOP measures, it is assumed that the users true positions and offset (x_u, y_u, z_u, t_u) can be computed by their approximate values $(\hat{x}_u, \hat{y}_u, \hat{z}_u, \hat{t}_u)$ and a displacement $(\Delta x_u, \Delta y_u, \Delta z_u, \Delta t_u)$ as:

$$\begin{aligned} x_u &= \hat{x}_u + \Delta x_u \\ y_u &= \hat{y}_u + \Delta y_u \\ z_u &= \hat{z}_u + \Delta z_u \\ t_u &= \hat{t}_u + \Delta t_u \end{aligned} \quad [9]$$

then, the pseudo-range equation can be linearized as:

$$\begin{aligned} & f(\hat{x}_u + \Delta x_u, \hat{y}_u + \Delta y_u, \hat{z}_u + \Delta z_u, \hat{t}_u + \Delta t_u) \\ &= f(\hat{x}_u, \hat{y}_u, \hat{z}_u, \hat{t}_u) + \frac{\partial f}{\partial \hat{x}_u}\Delta x_u + \frac{\partial f}{\partial \hat{y}_u}\Delta y_u + \frac{\partial f}{\partial \hat{z}_u}\Delta z_u + \frac{\partial f}{\partial \hat{t}_u}\Delta t_u \end{aligned} \quad [10]$$

where, defining $\hat{r}_i = \sqrt{(x_i-\hat{x}_u)^2 + (y_i-\hat{y}_u)^2 + (z_i-\hat{z}_u)^2}$:

$$\begin{aligned} \frac{\partial f}{\partial \hat{x}_u} &= -\frac{x_i-\hat{x}_u}{\hat{r}_i} = -a_{x_i} \\ \frac{\partial f}{\partial \hat{y}_u} &= -\frac{y_i-\hat{y}_u}{\hat{r}_i} = -a_{y_i} \\ \frac{\partial f}{\partial \hat{z}_u} &= -\frac{z_i-\hat{z}_u}{\hat{r}_i} = -a_{z_i} \\ \frac{\partial f}{\partial \hat{t}_u} &= c \end{aligned} \quad [11]$$

Therefore, the linearized pseudo-range equation can be written as:

$$\underbrace{\begin{pmatrix} \Delta\rho_1 \\ \Delta\rho_2 \\ \dots \\ \Delta\rho_n \end{pmatrix}}_{\Delta\rho} = \underbrace{\begin{bmatrix} \mathbf{a}_1 & 1 \\ \mathbf{a}_2 & 1 \\ \dots & \dots \\ \mathbf{a}_n & 1 \end{bmatrix}}_{\mathbf{H}} \underbrace{\begin{pmatrix} \Delta x_u \\ \Delta y_u \\ \Delta z_u \\ -c\,t_u \end{pmatrix}}_{\Delta\mathbf{x}} \quad [12]$$

where $\Delta\rho_i = \hat{\rho}_i - \rho_i$ and $\mathbf{a}_i$ is the unit vector pointing from the point P to the i-th satellite, S.

2.2.2 *DOP Figures*

The pseudo-range equation linearization corresponds to the Jacobian relating changes in the user position and time bias to changes in the pseudo-range values. If this relationship is inverted, it can be used to relate the covariance of the user position and time bias to the covariance of the pseudorange errors. The DOP parameters then are defined as geometry factors that relate parameters of the user position and time bias errors to those of the pseudo-range errors. Therefore, considering the general case where $n \geq 4$, Eq. 12, can be inverted as:

$$\Delta\mathbf{x} = \mathbf{K}\Delta\rho \quad \text{where} \quad \begin{matrix} \mathbf{K} = \mathbf{H}^{-1} \text{ if } n=4 \\ \mathbf{K} = \left(\mathbf{H}^\top\mathbf{H}\right)^{-1}\mathbf{H}^\top \text{ if } n>4 \end{matrix} \quad [13]$$

The matrix $\mathbf{K}$ is defined in Eq. 13 gives the functional relationship between the errors in the pseudo-range values and the induced errors in the computed position and time bias. This matrix, is a $4\times n$ matrix and depends only on the relative geometry of the user and the satellites participating in the least square solution computation.

The pseudo-range errors here are considered to be random variables. Therefore, Eq. 13 gives the functional relation between the random variables $d\mathbf{x}$ and $d\rho$. Assuming $d\rho$ identically distributed and independent and having a variance equal to the square of the satellite *User Equivalent Range Error* (UERE), it can be shown that [12]:

$$\mathrm{cov}(d\mathbf{x}) = \left(\mathbf{H}^\top\mathbf{H}\right)^{-1}\sigma^2_{\mathrm{UERE}} \quad [14]$$

Here the components of the matrix $\mathbf{Q} = \left(\mathbf{H}^\top \mathbf{H}\right)^{-1}$ quantify how pseudo-range errors translate into components of the covariance of $d\mathbf{x}$. Then, the different DOP measures can be defined exploiting $\mathbf{Q}$ and are useful to characterize the accuracy of various components of the position/time solution. In this study, Position Dilution of Precision (PDOP) and Horizontal Dilution of Precision (HDOP) are exploited, and are defined as:

$$\mathtt{PDOP} = \sqrt{Q_{11} + Q_{22} + Q_{33}} \quad [15]$$

$$\mathtt{HDOP} = \sqrt{Q_{11} + Q_{22}} \quad [16]$$

Note that for the computation of the HDOP, a minimum of 3 satellites in view instead of 4 can be used. Indeed, in this study:

- $\mathtt{HDOPAV}_j = \mathscr{F}_j(t,3)$ is used to identify the regions where the *HDOP* exists, and then its value is computed with Eq. 16;
- $\mathtt{DOPAV}_j = \mathscr{F}_j(t,4)$ is used to identify the regions where the *PDOP* exists, and then its value is computed with Eq. 15;

Therefore, the k-th region Mean iDOP availability is defined as the mean iDOP over a group of N_k surface points, such that:

$$\mathtt{mDOPAV} = \frac{1}{N_k} \sum_{j}^{N_k} \mathtt{DOPAV}_j \quad [17]$$

$$\mathtt{mHDOPAV} = \frac{1}{N_k} \sum_{j}^{N_k} \mathtt{HDOPAV}_j \quad [18]$$

In addition to that, a useful measurement of the navigation performances can be retrieved by evaluating the iDOP average performances over the time span when such measurements are available, leading to the following:

$$\mathtt{AVGDOP}_j = \frac{\int_{t_0}^{t_f} \mathtt{DOPAV}_j(\tau)\, \mathtt{PDOP}_j(\tau)\, d\tau}{t_f - t_0} \quad [19]$$

$$\mathtt{AVGHDOP}_j = \frac{\int_{t_0}^{t_f} \mathtt{HDOPAV}_j(\tau)\, \mathtt{HDOP}_j(\tau)\, d\tau}{t_f - t_0} \quad [20]$$

3. Optimisation Strategy

In order to ensure that the performances of the constellation of satellites satisfy the different requirements and provide thus a quality and reliable service, an optimisation procedure is putted in place. The exploitation of the principle of the well known Walker constellation architecture [9,20] can represent a plausible alternative if the goal of a specific constellation is to provide a coverage to the whole planetary surface, without any regional distinction. If instead specific regions have to be targeted, the Walker constellation results in an unnecessary over-dimensioning of the constellation. Indeed, generally speaking, to ensure good performances to a specific region, the same performances are also guaranteed to the rest of the surface, leading the total number of needed constellation spacecraft to sky-rocket. On the other side, setting up an optimisation problem can be exploited to retrieve an efficient, and yet effective, constellation configuration to prioritize the desired performances on specific regions.

Moreover, it may happen that the goal of the constellation is declined to a set of specific figures of merit, which may in general have clashing behaviours, due also to the application of the former to different regions of the user volume. As a consequence, using a single objective optimisation routine cannot be done without the need of exploiting as cost function a weighted sum of the various indexes. This strategy ha been proved effective for many optimisation problems, but it may not be the case for such specific case, due to the impossibility to provide a-priori weights to the different performances. Moreover, there are a number of well-known drawbacks of the weighted sum method [3,16]: in fact, often the optimal solution distribution is not uniform, and that the optimal solutions in non-convex regions are not detected. Therefore, a *Multi-Objective Optimisation* (MOO) strategy is exploited [18].

In the following paragraphs the optimisation strategy for the constellation design is presented, highligthing the different regions of users to be targeted, the various variable of design involved in the orbit selection and the specific definition of the objectives of the optimisation.

3.1 *Genotype*

The MOO genotype is built in such a way that a constellation with N Keplerian Orbits is constructed. In particular, the design variables space has been defined as:

- N: number of constellation elements, *fixed a-priori*;
- Semi-major axis (`sma`), eccentricity (`ecc`), inclination (`inc`) and pericenter anomaly (`aop`) are considered to be the same for the whole constellation element: the orbit semi-major axis is *fixed a-priori* to 9750.7 km, in order to ensure a period of 24 hours, while `ecc`, `inc` and `aop` are considered to be the same of all the elements in the constellation - this choice is performed since the constellation deployment will benefits from having orbits with the same shape and on planes with the same inclination.
- RAAN (`ran`) and true anomaly (`tan`) are optimised for every i-th constellation element.

Hence, the design variables vector **x** is defined as:

$$\mathbf{x} = (\texttt{ecc}, \texttt{inc}, \texttt{aop}, \texttt{ran}_i, \texttt{tan}_i)^\top \quad i = 1, \ldots, n \quad [21]$$

with a total number of $3+2n$ variables.

3.2 *Geographical Sampling*

Surface Users In order to provide the possibility to assess the performances towards different Moon users, three different regions on the Moon surface have been identified by discerning the latitude λ, as highlighted by Fig. 1 and described hereafter.

1. *South Pole* (SP) : $-90° \leq \lambda \leq -70°$. The region around the South Pole, where many of the future Lunar exploration missions will be targeted.
2. *Equatorial* (EQ) : $-70° \leq \lambda \leq 70°$. This region represents all the points within a band of 140° centred in the equator.
3. *North Pole* (NP) : $70° \leq \lambda \leq 90°$. The remaining region, covering the neighborhood of the North Pole.

Orbital Users Orbital users may also benefit from the constellation services. A dedicated numerical simulation as been performed to asses the influence of the altitude over the Lunar surface in the performances of the constellation. A constellation of *five*, 24 hours, Elliptical Lunar Frozen Orbits is considered in this analysis [17], distributing the constellation orbiters over three orbital planes with an inclination of 63°. This configuration is considered as a good alternative for South Pole services performances.

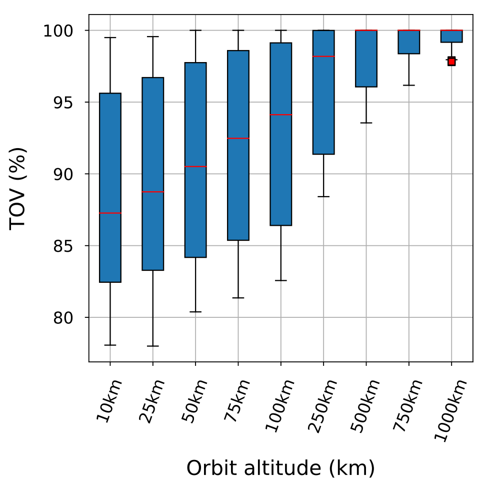

Fig. 2: `TOV` ranges as a function of the orbit altitude.

In Fig. 2 are presented the results of the `TOV` ranges associated to circular orbits at different altitudes: it is evident that the lower the altitude the higher the `TOV` dispersion is higher as well as the mean value (red line in the plot) is lower. The same trend is highlighted by performing a similar analysis on the mean `AVGDOP` among the different users. Thus, surface users provide the worst case condition and can be used for the optimisation, reducing the computational effort for the evaluation of the cost function.

3.3 *Time of Simulation*

An additional analyses required in order to ease the computational burden on the cost function evaluation represents the simulation time employed. The effect on the `TOV` and on the average number of satellites in view (i.e. the time-average of $\mathcal{N}_j(t)$) for different latitudes has been addressed by changing the final time of the simulation from a minimum of 1 month up to 12 months. Figure 3 represents the analysis performed on the `TOV`.

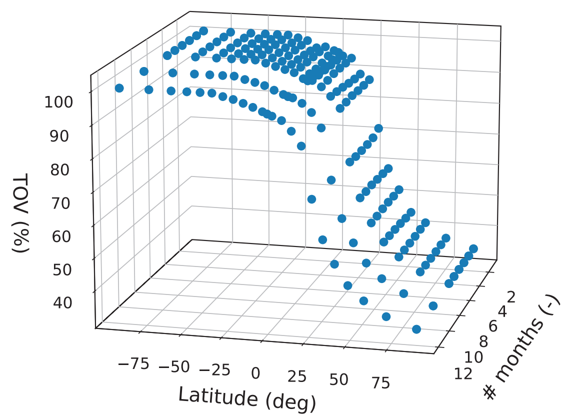

Fig. 3: `TOV` ranges for different users' latitudes as a function of the number of simulated months.

It is clearly visible that the results do not vary consistently and significantly by exploiting a simulation time of 1 or 12 months, indistinctly from the users' latitude. Such behaviour is not different by looking at the average number of satellites in view for different latitudes users. As a consequence, a total simulation time on 1 month has been exploited for the computation of the cost function.

3.4 *Cost Function Objectives*

In order to showcase the flexibilty and versatility of the proposed constellation design strategy, two different optimisation paths have been followed, based on the necessity or not to exploit the differentiation between the three regions. In particular, a first run with 5 objectives has been put in place with the idea of providing optima for specific sub regions. Secondly, a run with just three objectives associated to the whole surface has been performed. Table 1 and 2 describe the various objectives for the regional and whole surface optimisations respectively.

Objectives	Formulation	for j in
TOV_SP	1-min($\mathtt{TOV}_j$)	SP
HDOPAV_SP	1-min($\mathtt{HDOPAV}_j$)	SP
AVGHDOP_SP<5	1-min($\mathtt{AVGHDOP}_j$<5)	SP
TOV_EQ	1-min($\mathtt{TOV}_j$)	EQ
TOV_NP	1-min($\mathtt{TOV}_j$)	NP
HDOPAV_EQNP	1-min($\mathtt{HDOPAV}_j$)	EQ, NP

Table 1: Regional Moon surface optimisation objectives

Objectives	Formulation	for j in
TOV	1-min($\mathtt{TOV}_j$)	SP, EQ, NP
HDOPAV	1-min($\mathtt{HDOPAV}_j$)	SP, EQ, NP
AVGHDOP<5	1-min($\mathtt{AVGHDOP}_j$<5)	SP, EQ, NP

Table 2: Overall Moon surface optimisation objectives

In addition to the already presented indexes of the $\mathtt{TOV}_j$ and the $\mathtt{HDOPAV}_j$, a measurement of the HDOP performances themselves has been included. Looking for a specific threshold value of 5, under which the HDOP performances are considered to be excellent, the percentage of time in which this value is met by a single j-th user is identified by the symbol $\mathtt{AVGHDOP}_j$<5. These three involved quantities are all parameters to be maximised. As such, the minimum value recorded over the whole surface region under interest is taken to construct the cost function, and, in order to have objectives to be minimised, its complementary value to 1 is used.

Having distinguished between a regional and a non-regional optimisation run, it is expected to be able to retrieve solutions with different properties. Indeed, from the regional one, it will be possible to extract solutions with very high performances on specific objectives while presenting extremely bad behaviours in other ones. On the contrary, the best solutions out of the non-regional optimisation will provide moderate to good performances hopefully to all the involved user regions.

4. Optimisation Analysis & Results

In general, the multi-objective optimization can be stated as follows:

$$\min \mathbf{J}(\mathbf{x},\mathbf{p}) \quad \text{s.t.} \quad \begin{aligned} \mathbf{g}(\mathbf{x},\mathbf{p}) &\leq 0 \\ \mathbf{h}(\mathbf{x},\mathbf{p}) &= 0 \\ \mathbf{x} &\in (\mathbf{x}_{LB},\mathbf{x}_{UB}) \end{aligned} \qquad [22]$$

where the objective function vector $\mathbf{J}$, whose elements are reported in Table 1 for the *regional* problem or in Table 2 for the whole surface one, is a function of design variables vector $\mathbf{x}$, which is described in Section 3.1, and a fixed parameter vector $\mathbf{p}$; $\mathbf{g}$ and $\mathbf{h}$ are inequality and equality constraints and $\mathbf{x}_{LB}$ and $\mathbf{x}_{UB}$ are the lower and upper bounds for the design variables.

In this study, none between equality and inequality constraints are imposed out of the cost function, therefore $\mathbf{g} = \emptyset$ and $\mathbf{h} = \emptyset$. The optimisation parameters, $\mathbf{p}$, are instead:

$$\mathbf{p} = (\mathtt{sma}, N, \Delta T)^\top \qquad [23]$$

where sma is the orbits semi-major axis, N the number of orbiters and ΔT the simulation time window. Here, the optimisation bounds are set to:

$$\mathbf{x}_{LB} = (0,0,0,[0]\times 2N)^\top$$
$$\mathbf{x}_{UB} = (0.7,90,360,[360]\times 2N)^\top$$

The exploration of the design variable space and the generation of the Pareto fronts for both the optimisation run are performed through the exploitation of a *Multi-Objective Hypervolume-Based Ant Colony Optimisation* (MHACO) algorithm [1]. The ESA *pagmo* [2] optimisation package has been exploited for that purpose. MHACO is preferred over standard heuristic methods, such as the *Non-Dominated Sorting Particle Swarm Optimiser* (NSPSO) [15] or the *Non-Dominated Sorting Genetic Algorithm* (NSGA-II) [4], since it is shown to be really competitive with those algorithms, exhibiting superior performances in large search space exploration.

After a preliminary analysis, a population of 60 elements and a maximum number of 250 evolution are considered. Three different optimisation runs have been performed for both the problems, considering a number of satellites N of 3, 4 and 5 respectively, while keeping fixed the other remaining parameters, sma and ΔT to 9750.7 km and 1 month respectively.

4.1 *Pareto Front Analysis*

From the optimisation routines, a population of 60 alternatives is extracted and, in order to visualise the feasibility boundaries of constellation with the different values of N. The results of the regional optimisation run are shown in Fig. 4. Although at first glance this set of charts might be confusing, it can be interpreted by looking it as a collection of sub-Pareto fronts, comparing the performances of the 60 alternatives two objectives per time. By looking closely to a specific row or column of the grid, it is possible to extract the obtainable performances for a specific objective. E.g., examining the TOV_SP row, it is possible to see that a minimum value of roughly 50% is obtained (in this case by a constellation of 3 servicers), while the maximum value can reach 100% for $N = 5$ and $N = 4$.

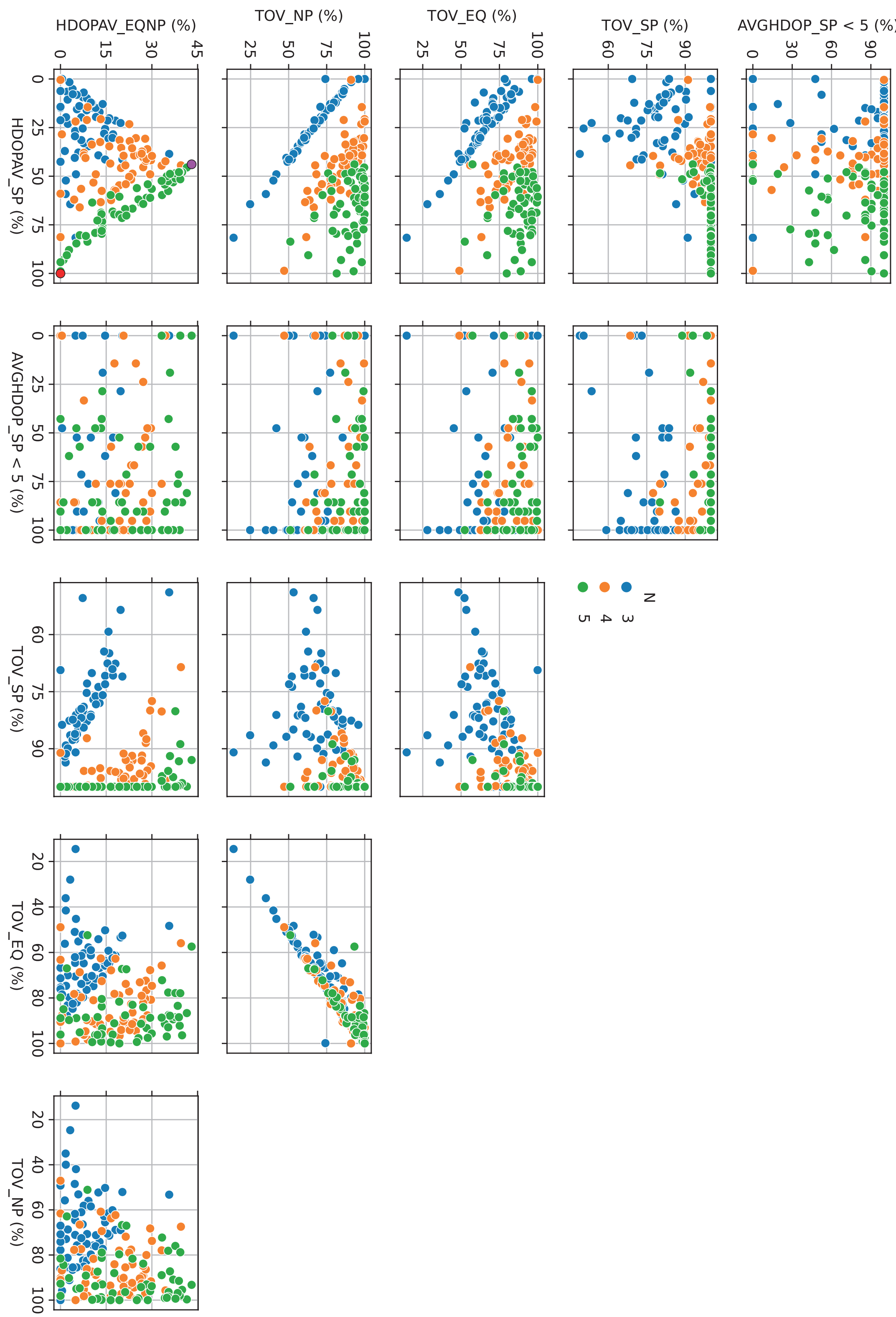

Fig. 4: Pareto front plots for the regional optimisation run. The extracted configurations are highlighted in the bottom left plot. The red dot identifies solution A, optimal for the South Pole `HDOPAV`, while the purple one represents solution B, optimal for the rest of the surface `HDOPAV`.

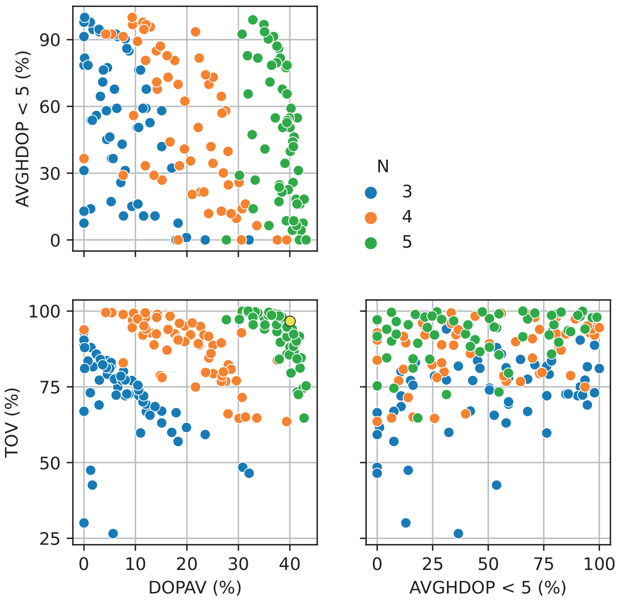

Fig. 5: Pareto front plots for the non-regional optimisation run. The extracted configuration of solution C is represented by a yellow dot in the bottom left plot.

As a general remark, one can see that with $N = 3$ there are none providing 100% of navigation service availability in neither SP nor EQNP regions, while solutions with 100% of communication availability in specific regions are possible. Among N = 5 solutions it is possible to find solutions with both communication and navigation services regionally available to the 100% of the users. Solutions with $N = 4$

Considering the constellation design procedure, the chart in the bottom left which relates the `HDOPAV_SP` and the `HDOPAV_EQNP` performances is of primary importance. Two specific solutions with $N = 5$ are extracted from here, that will be called *Solution A* and *Solution B*, identified in Fig. 4 with a red and purple dots respectively. The former is taken as the optimal solution for the navigation service availability at the South Pole, reaching a value of 100% of `HDOPAV_SP`, whilst providing the extremely poor performances of 0% in `HDOPAV_EQNP`. The contrary is instead obtained for the latter solution, where the performances in `HDOPAV_SP` are penalised (reaching 44%) to enhance instead the `HDOPAV_EQNP` performance to its maximum obtainable with $N = 5$, i.e. 43%.

Figure 5 presents instead the results for the non-regional optimisation run, where, being the number of objectives reduced to three, much more readable charts are available. In particular, a clear Pareto front is visible in the `TOV–DOPAV` plot, where it is possible to see that solutions with 100% of communication availability all over

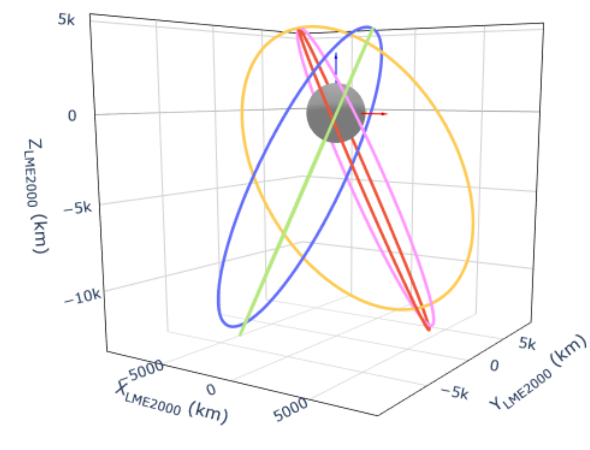

Fig. 6: Orbital representation of the A alternative, optimised for the navigation performances on the South Pole.

the globe are possible with $N = 4, 5$, while the maximum values for the navigation availability is around 45%, with $N = 5$.

The alternative highlighted by a yellow dot, called *Solution C* is extracted as the knee point of the population. This is defined as the point with the lowest distance to the *utopia point*, i.e. the utopic condition of reaching the highest possible performances on all the objectives, represented in this case by the point with 100% in all the indexes. Such point represent the best compromise for all the objectives, presenting a score close to the maximum for each one, i.e. 37% for `HDOPAV`, 37% for `AVGHDOP<5` and 98% for `TOV`.

A visual representation of the three constellations alternatives can be seen in Fig. 6, 7 and 8, for A, B and C respectively, where the orbits of the various satellite are displayed in an inertial reference frame centred in the Moon.

4.2 *Constellation Robustness*

The Pareto front analysis gave the possibility to select what will be a good performances for specific regions, however there are some operational aspects that may need to be addressed. In particular, a critical analysis on the constellation tolerance to failures of a single orbiter may be useful.

In such perspective, the performance of the three extracted solutions have been computed by letting one constellation satellite per time out of the constellation. Thus, a total of five simulations per each configuration have been performed and the worst performances in each of the optimisation objectives are recorded in order to anal-

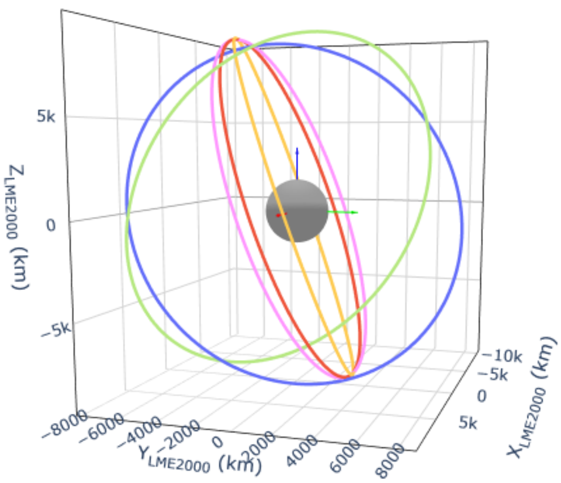

Fig. 7: Orbital representation of the B alternative, optimised for the navigation performances on the Equatorial region and the North Pole.

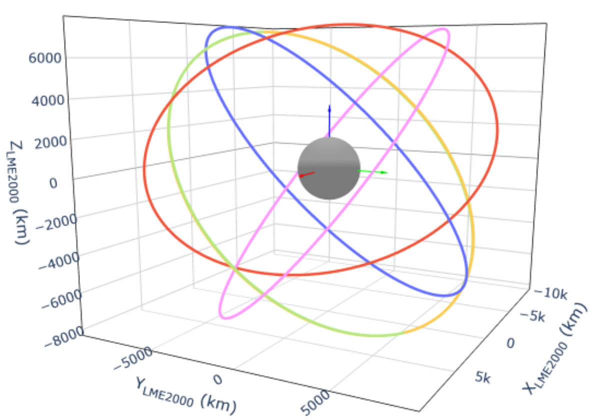

Fig. 8: Orbital representation of the C alternative, optimised for both communication and navigation performances on the whole Moon surface.

yse which worst case conditions may occur by the failure of a single object.

The obtained results are reported in Table 3 and 4 for the solutions A and B and C respectively. For sake of simplicity the complementary to 1 of the various cost function components are reported, so, optimal values are towards 100%, while poor ones tend to 0%.

Objective	A	A fail	B	B fail
1-HDOPAV_EQNP (%)	0	0	43	0
1-HDOPAV_SP (%)	100	50	44	3
1-AVGHDOP<5_SP (%)	100	0	0	0
1-TOV_SP (%)	100	99	93	51
1-TOV_EQ (%)	80	39	57	52
1-TOV_NP (%)	82	39	93	53

Table 3: Worst case performances of A and B solutions without and with failure of a single orbiter.

Objective	C	C fail
1-HDOPAV (%)	37	2
1-AVGHDOP<5 (%)	91	0
1-TOV (%)	98	49

Table 4: Worst case performances of C solution without and with failure of a single orbiter.

In all cases, the resulting performances are drastically reduced from the starting point, for both the regional and non-regional solutions. The only exception is represented by the availability of the SP-region Communication service for the South Pole optimised constellation, i.e. the TOV_SP index for the solution A, whose performances see a reduction of 1% only. Similarly also solution B show a drop by just 5% in the TOV_EQ index. For the Navigation related performances drops by more than 40% are recorded in all the solutions, with peaks above 90% for the AVGHDOP<5 indeces.

It is possible then to conclude from such analysis that regional specific optima can be quite robust towards the communication related performances. This is not the case for the non-regional optimisation and in general for all the navigation related indexes. To increase the robustness of the constellation towards a single orbiter failure, the definition of specific cost function objectives can be introduced, with the aim of performing dedicated optimisation runs and include an additional plot on the Pareto front grid.

5. Constellation Enhancement

Spacecraft flying in a non-Keplerian orbiting regime have been proven to be extremely effectively for various different purposes [7].

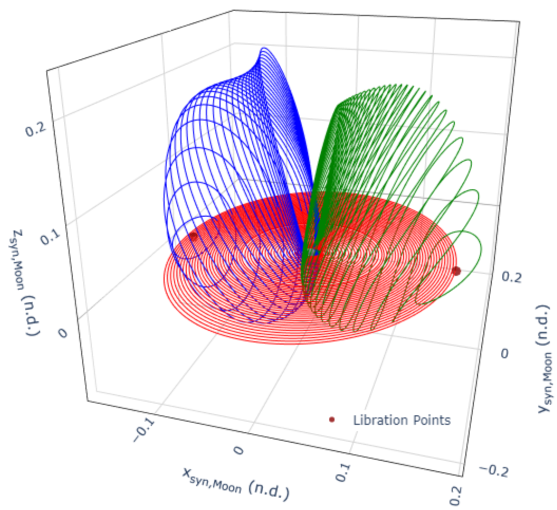

Fig. 9: Non-Keplerian orbital families considered in the Earth-Moon non-dimentional rotating coordinates, centred at the Moon: DRO family in red, NHL1 in blue and NHL2 in green.

In Fig. 9, for the different orbital families, the set of available orbits have been plotted in the Earth-Moon synodic reference frame which is able to derive extremely relevant feature, due to its peculiarities. Firstly, it is possible to obtain hints on the Earth visibility, since the Earth-Moon configuration is fixed in this frame. Moreover, the Moon attitude is almost fixed in such frame, due to the almost tidal lock of the natural satellite with respect to the Earth, allowing the a-priori prediction of visibility patterns of each orbit on the Moon surface regions.

The possibility of exploiting such features also for enhancing the constellation performances is a promising idea which is analysed in this Subsection. Keeping the attention on solution A only, which satisfies completely the service requirements for the SP region, the idea of this analysis is to find which additional orbiters may be added to increase the most the performances in the remaining surface regions. The orbital families in the non-Keplerian environment to be exploited are then reduced a subset of three: *Distant Retrograde Orbits* (DRO) and *Northern Halo Orbits* in L_1 and L_2 (NHL1, NHL2). The former can indeed be exploited for adding a relevant contributions to the objectives associated to the equatorial region. The other two families can instead cope with the lack of visibility of the North Pole by the Keplerian base

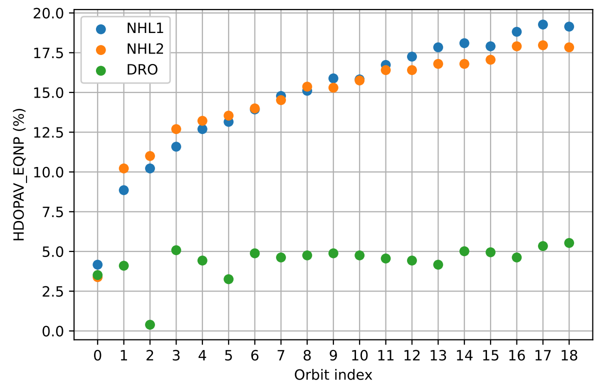

Fig. 10: Evolution of the `HDOPAV_EQNP` performance as function of the orbit index, for the different proposed families, i.e. DRO, NHL1 and NHL2.

of solution A, which was optimised for the antipodal region of the Moon. Moreover, orbits of the NHL1 family and many also among the largest ones in the NHL2 family present a continuous Earth visibility, which is a key feature for providing communication relay services.

5.1 *Addition of a Single Orbiter*

The performance of the enhanced constellations are evaluated by letting the orbits in the various families vary with an associated index, going from `0` to `18`, staring thus from smaller orbits with lower indexes and increasing more and more its amplitude, as visible in Fig. 9.

Figure 10 presents the evolution of the `HDOPAV_EQNP` index as function of the different orbit ID for the three proposed families. From such plot, it is possible to extract the fact that the inclusion of the DRO can increase at most by 5% the performance, almost independently by the orbit amplitude. This is not the case instead for the NHL1 and NHL2 families, where increasing the amplitude, and thus the out-of-plane component of the Halo, a consistent increase in the index is recorded, approaching the value of 20%. The other two indexes, which are `TOV_EQ` and `TOV_NP` present an increment of up to 16% with respect to the values of the pure keplerian A solution, approaching for the NHL1 and NHL2 case 98%.

5.2 *Addition of Two Orbiters*

Given that the increment in performances with the addition of a single non-Keplerian orbiter were not able to increase consistently the navigation availability in the EQ and NP regions, the addition of another orbiter has been taken into account. For this further analyses, we chose to exploit directly a single orbiter from the NHL1 and another from the NHL2 given the results obtained by the

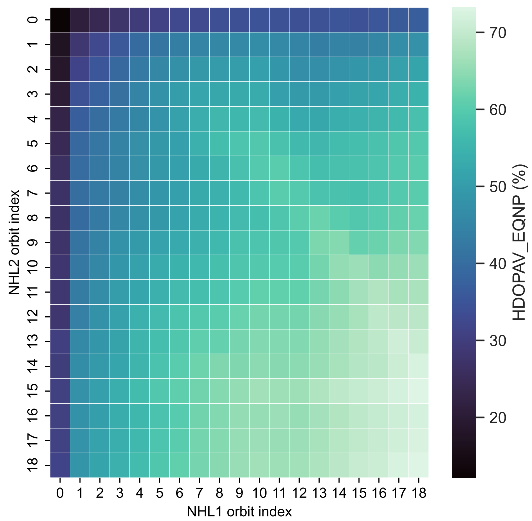

Fig. 11: Evolution of the HDOPAV_EQNP performance as function of the orbit index of the two orbiters to be added, taken from the NHL1 and NHL2 families.

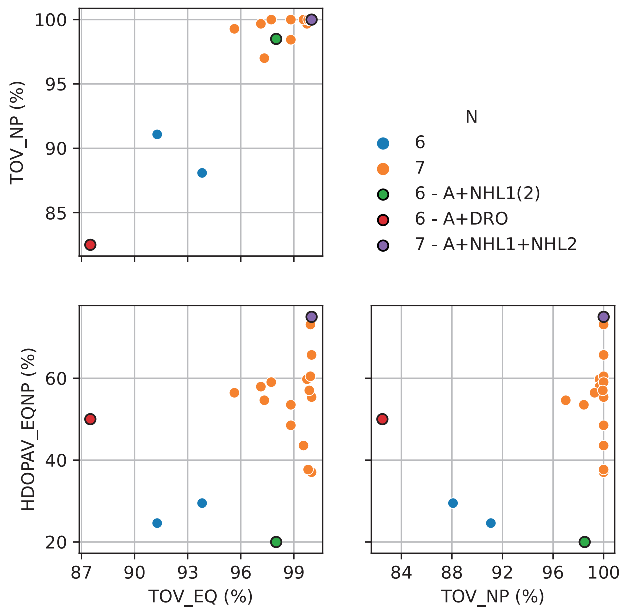

Fig. 12: Pareto plots for the alternatives with $N = 6$ and $N = 7$, presenting the solutions of the fully Keplerian optimised populations (satisfying by 100% the constraints associated to the SP region) on the scores in the EQ and NP regions. Solutions from the hybrid constellations are overlapped for comparisons.

single orbiter addition analysis. Figure 11 shows the results in the form of an heatmap representing also in this case the HDOP_EQNP value.

As expected by the trend of Fig. 10, the best solution is obtained by exploiting also in this case the highest index orbits. The optimal solution is able to increase the performance index to a value of 75%, while both the communication related indexes reach the value of 100%.

5.3 *Comparison with fully Keplerian constellations*

In order to compare the results of such configurations with the addition of orbiters in the non-Keplerian regime to the obtainable results of a fully Keplerian constellation, additional optimisation runs with the regional cost function fixing $N = 6$ and $N = 7$ have been performed.

Figure 12 presents all the elements of the populations of $N = 6$ and $N = 7$ that, similarly to solution A, satisfy completely by 100% the three performance indexes in the SP region. Only the indexes associated to the EQ and NP regions are thus displayed in the grid.

On the Pareto plots, also the three solutions associated to the hybrid constellations are reported, i.e. the addition of an orbit from the NHL1(or NHL2) family (green dot), the addition of a DRO (red dot) and of one orbiter from both the NHL1 and the NHL2 family (purple dot). From that it is possible to see that the performance of the green dot (A + NHL1(2)) are able to outperform the best candidate for the fully Keplerian constellation with $N = 6$ (hereafter called *Solution D*. Similar conclusions can be drawn in the comparison of the constellations with $N = 7$. Also here, the solution of the hybrid constellation is able to provide better or comparable performance than the fully Keplerian (*Solution E*), in particular showing higher values of the navigation availability score.

The overall performances of the different proposed alternatives are summarised in Table 5.

From here it is possible to directly map the different performance increments obtained by hybrid constellations with respect to the starting configuration of solution A. Moreover, also the results of the solutions optimised directly with $N = 6$ and $N = 7$ are reported, highlighting the benefits that a hybrid configuration can have with respect to a completely Keplerian one.

6. Conclusions & Future Works

The current paper has presented a novel versatile approach towards the design of optimised hybrid satellite constellations with the goal of providing Communication and Navigation services to the future Moon exploration missions. The goal of encapsulating different performance indexes associated to different specific user regions has been achieved by employing a Multi-Objective

Objective	A	+DRO	+NHL1
`1-HDOPAV_EQNP (%)`	0	50	20
`1-TOV_EQ (%)`	80	88	98
`1-TOV_NP (%)`	82	83	98
Objective		+NHL2	+NHL1/2
`1-HDOPAV_EQNP (%)`		20	75
`1-TOV_EQ (%)`		98	100
`1-TOV_NP (%)`		98	100
Objective		D	E
`1-HDOPAV_EQNP (%)`		28	73
`1-TOV_EQ (%)`		94	100
`1-TOV_NP (%)`		88	100

Table 5: Comparison of obtainable performances for EQ and NP regions of the different proposed constellation configurations with both hybrid and fully Keplerian solutions.

Optimisation strategy. In such a manner, it is possible to retrieve a set of optimal and non-dominated solutions with respect to some specific parameters (e.g. the number of constellation satellites) and analyse them in Pareto front plots, in order to explore the space of feasibility. From such plots, one can extract optima for specific objectives or optimal knee points on the Pareto front.

In this study three solutions have been analysed: one optimised for the navigation service on the South Pole, one on the rest of the surface and a last one finding a compromise on the whole Moon surface. The three alternatives have been analysed also for robustness against a single satellite failure showing the optimisation of performances in specific regions can increase the reliability in this non-contingency scenario, with respect to what happens for non-regional optima. Lastly, the effects of adding non-Keplerian orbiting satellites to the optimised basis have been described, highlighting which families in the Cislunar environment are more prone to such objective. To summarize those results, in Fig. 13 the different alternatives major performance indexes (i.e. `TOV` and `HDOPAV`) are presented compared as function of the Moon latitude, for the regional cases. In particular:

- Solution *A* represents a Pareto optimal solution for South-Pole related performances, but with the addition of 1 or 2 satellites in Keplerian or non-Keplerian regimes, the regional coverage is extended to the rest of the surface.

- Solution *B* represents a compromise between South-Pole and Equator/North-Pole `HDOPAV`, therefore ex-

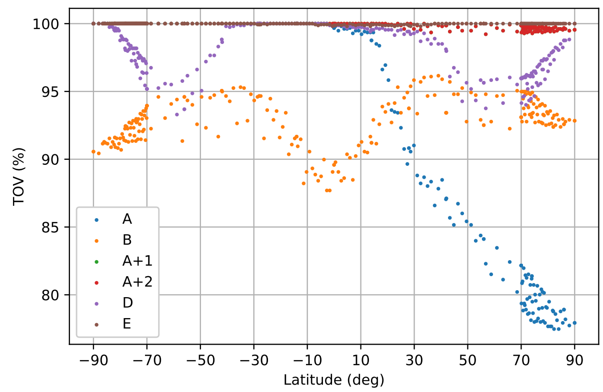

(a)

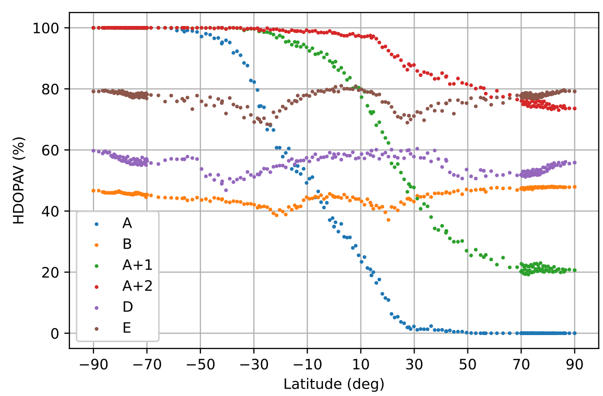

(b)

Fig. 13: Constellation performance indexes as function of the Moon latitude, λ.

hibits approximately the same (moderate) performances independently on the latitude.

- The addition of Keplerian or Non-Keplerian orbits brings approximately the same benefits from the TOV/HDOPAV point of view. However, the exploitation of Libration Points Orbits could be beneficial for other operative aspects: the continuous visibility of the Earth or of specific lunar regions (the Far Side, for example, in case of L_2 LPOs).

Among the possible additional studies in this framework, two main points could be addressed. Firstly, as highlighted in the robustness analysis, the performances overall degrade by far, especially for the navigation services. As such, the possibility to include such robustness analyses in the optimisation architecture would be an added key element. Moreover, the capability to add platform-related constraints to the optimization (e.g. maximum slant range, minimum masking angle, ...) can be fundamental parts to help the spacecraft system design process and ease the whole definition of the infrastructure as a whole.

7. Acknowledgements

The research is in the field of the on-going Politecnico di Milano studies on ESA-TIA-T-SOW-0181 13/11/20. The authors would like to acknowledge the whole LCNS team under the Moonlight programme financed activities.

References

[1] Giacomo Acciarini, Dario Izzo, and Erwin Mooij. Mhaco: a multi-objective hypervolume-based ant colony optimizer for space trajectory optimization. In *2020 IEEE Congress on Evolutionary Computation (CEC)*, pages 1–8, 2020.

[2] Francesco Biscani and Dario Izzo. A parallel global multiobjective framework for optimization: pagmo. *Journal of Open Source Software*, 5(53):2338, 2020.

[3] Indraneel Das and John E Dennis. A closer look at drawbacks of minimizing weighted sums of objectives for pareto set generation in multicriteria optimization problems. *Structural optimization*, 14(1):63–69, 1997.

[4] Kalyanmoy Deb, Amrit Pratap, Sameer Agarwal, and TAMT Meyarivan. A fast and elitist multiobjective genetic algorithm: Nsga-ii. *IEEE transactions on evolutionary computation*, 6(2):182–197, 2002.

[5] Jessica Flahaut, J Carpenter, J-P Williams, M Anand, IA Crawford, W van Westrenen, E Füri, L Xiao, and S Zhao. Regions of interest (roi) for future exploration missions to the lunar south pole. *Planetary and Space Science*, 180:104750, 2020.

[6] Mark Flanegan, Jonathon Gal-Edd, Lynn Anderson, Joseph Warner, Todd Ely, Charles Lee, Biren Shah, Arvydas Vaisnys, and James Schier. Nasa lunar communication and navigation architecture. In *SpaceOps 2008 Conference*, page 3589, 2008.

[7] Daniel J Grebow. *Trajectory design in the Earth-Moon system and lunar South Pole coverage*. PhD thesis, Purdue University, 2010.

[8] Daniel J Grebow, Martin T Ozimek, Kathleen C Howell, and David C Folta. Multibody orbit architectures for lunar south pole coverage. *Journal of Spacecraft and Rockets*, 45(2):344–358, 2008.

[9] Meiqian Guan, Tianhe Xu, Fan Gao, Wenfeng Nie, and Honglei Yang. Optimal walker constellation design of leo-based global navigation and augmentation system. *Remote Sensing*, 12(11):1845, 2020.

[10] Kathryn Hamera, Todd Mosher, Mark Gefreh, Robert Paul, Leon Slavkin, and Joseph Trojan. An evolvable lunar communication and navigation constellation concept. In *2008 IEEE Aerospace Conference*, pages 1–20. IEEE, 2008.

[11] David J Israel, Kendall D Mauldin, Christopher J Roberts, Jason W Mitchell, Antti A Pulkkinen, D Cooper La Vida, Michael A Johnson, Steven D Christe, and Cheryl J Gramling. Lunanet: a flexible and extensible lunar exploration communications and navigation infrastructure. In *2020 IEEE Aerospace Conference*, pages 1–14. IEEE, 2020.

[12] Elliott D Kaplan and Christopher Hegarty. *Understanding GPS/GNSS: principles and applications*. Artech house, 2017.

[13] Wang Sang Koon, Martin W Lo, Jerrold E Marsden, and Shane D Ross. Dynamical systems, the three-body problem and space mission design. In *Equadiff 99: (In 2 Volumes)*, pages 1167–1181. World Scientific, 2000.

[14] Kathleen C Laurini, Bernhard Hufenbach, Junichiro Kawaguchi, Jean-Claude Piedbœuf, Britta Schade, Jeremy Curtis, and H Kim. An international strategy for human exploration of the moon: the international space exploration coordination group (isecg) reference architecture for human lunar exploration. In *Proceedings of the 61st International Astronautical Congress*, pages 1–9. International Astronautical Federation (IAF) Paris, 2010.

[15] Xiaodong Li. A non-dominated sorting particle swarm optimizer for multiobjective optimization. In Erick Cantú-Paz, James A. Foster, Kalyanmoy Deb, Lawrence David Davis, Rajkumar Roy, Una-May O'Reilly, Hans-Georg Beyer, Russell Standish, Graham Kendall, Stewart Wilson, Mark Harman, Joachim Wegener, Dipankar Dasgupta, Mitch A. Potter, Alan C. Schultz, Kathryn A. Dowsland, Natasha Jonoska, and Julian Miller, editors, *Genetic and Evolutionary Computation — GECCO 2003*, pages 37–48, Berlin, Heidelberg, 2003. Springer Berlin Heidelberg.

[16] Achille Messac and Christopher A Mattson. Generating well-distributed sets of pareto points for engineering design using physical programming. *Optimization and Engineering*, 3(4):431–450, 2002.

[17] Miriam Schonfeldt, Antoine Grenier, Anaïs Delépaut, Pietro Giordano, Richard Swinden, Javier Ventura-Traveset, Daniel Blonski, and Jörg Hahn. A system study about a lunar navigation satellite transmitter system. In *2020 European Navigation Conference (ENC)*, pages 1–10. IEEE, 2020.

[18] Wolfram Stadler. *Multicriteria Optimization in Engineering and in the Sciences*, volume 37. Springer Science & Business Media, 1988.

[19] V. Szebehely. *Theory of Orbits: The Restricted Problem of Three Bodies*. Academic Press, New York and London, 1967.

[20] John G Walker. Satellite constellations. *Journal of the British Interplanetary Society*, 37:559, 1984.

[21] Don E Wilhelms, Keith A Howard, and Howard Gordon Wilshire. *Geologic map of the south side of the Moon*. Department of the Interior, US Geological Survey, 1979.